Supporting information

S1. Recovery of graphite from spent Li-ion batteries (LIB) and synthesis of graphite oxide (GO)

The spent LIBs were collected from different sources and dismantled with care to obtain the graphite, which is generally found to be coated on copper foil (anode of LIBs). This graphite coated on the Cu-foil is carefully scraped out in such a way that the copper foil is not mixed with the scrapings. The batteries from which the graphite was recovered were Nokia BL-4C and BL-5C. Thus, graphite was attained without any further purification and was used for the synthesis of GO following modified Hummer's method.

In Hummer's method [1] of GO synthesis, 1 g of recovered graphite powder was added to a mixture of 40 mL of conc. H_2SO_4 and 10 mL of conc. H_3PO_4 was taken in a 500 mL beaker, to which 1 g $NaNO_2$ was added, and the content was stirred at 50 °C. During stirring 6 g of $KMnO_4$ was added to it pinch-wise. The stirring and heating were continued for 12 h. After 12 h, the reaction product was slowly transferred into a 1 L beaker containing ice cubes with constant stirring using a glass rod, and 30 mL of 6% H_2O_2 was added and stirred well. Eventually, the product was washed several times with distilled water, centrifuged, and dried; this GO was used for the synthesis of GC.

In the case of the synthesis of GPGC, the GO synthesized using the pristine graphite instead of recovered graphite was used.

S2. Fabrication

The as-synthesized GC and GPGC were fabricated as symmetric supercapacitor devices following the method reported in [4,5]. In this procedure, a pair of carbon fabric of dimensions 2 cm × 2 cm was coated with electrode material by drop casting, a Whatman filter paper (Cat.

No.-1001 125) (2 cm × 2 cm) was used as a dielectric material, and a pair of stainless-steel plates nearly of same dimensions of carbon fabric are used as current collectors.

S3. Characterizations and measurements

The IR spectra of GC and GCPG were recorded using the ATR setup of FT-IR Perkin Elmer spectrophotometer (brand- L1600300 Spectrum TWO LiTa(serial No.- 117460)). The powder–XRD spectra (Rigaku D/teX Ultra 250 diffractometer) using Cu Kα (λ=1.54 Å) at 40 kV and 200 mA, FE-SEM images and EDS spectra were recorded using a field emission spectroscope (Carl Zeiss Strasse 22) and EDAX (model – ELECT PLUS (serial No.:31261), respectively. The BET surface analyses were carried out using the Qyantachrome surface area and pore size analyzer (model- Autosorb iQ-XR-XR-XR (3 Stat.) Viton (serial No.: 1050041616) at 77 K with N_2 adsorbate and the pretreatment of degassing was conducted at 200 °C for 8 h**.** Raman spectra were recorded (400–4000 cm^{-1}) using Horiba Yvon Jobin microscope (Labram hr800, wavelength of laser-532 nm). Electrochemical characterizations of electrode material were carried out at a potential range of 0-1.2 V by cyclic voltammetry (CV), galvanostatic charge/discharge (GCD) and electrochemical impedance spectroscopy (EIS) (frequency range of 100 kHz - 0.01 Hz at open circuit potential with an AC perturbation amplitude of 10 mV) using two electrode systems with 1 M H_2SO_4 as the electrolyte (Ametek-VersaSTAT3 (Princeton Applied Research)).

Crystallite size (L) (in nm) [3]

$$L = \frac{k\lambda}{b\cos\theta} \qquad \text{(S1)}$$

k = 0.94 (Scherrer constant) and b= full width half maxima of the diffraction peak.

Number of graphene layers per domain or crystallite [2]

$$n = \left(\frac{D}{d} + 1\right) = \left(\frac{2Kta}{\beta} + 1\right) \qquad \text{(S2)}$$

Where, D= the average crystalline width and d = interplanar distance,

$$D = \frac{K\lambda}{\beta \cos\theta} \qquad \text{(S3)}$$

Where, K = constant related to a crystallite shape, normally taken as 0.89 for spherical crystal with cubic unit cells, β = Full-width half maxima (FW-HM) in radians, and λ = wave length of CuKα (1.54 Å)

Specific capacitance (C_s in F g^{-1}) of a supercapacitor device [3–5]

$$C_s = \frac{I}{m\frac{dV}{dt}} \qquad \text{(S4)}$$

where, I is the constant current (in A), m is the total mass of the two electrodes (in g), dV/dt in V s^{-1}) is the slope obtained by fitting a straight line to the discharge curve over the range of V (the voltage at the beginning of discharge after correcting for IR drop).

Specific capacity (Q in C g^{-1})

$$Q = C_s \times \Delta V \qquad \text{(S5)}$$

where, C_s is the specific capacitance (F g^{-1}) and ΔV is the potential window used.

Specific energy (E_s in W h kg^{-1})

$$E_s = \frac{1000 \times C_s \times (\Delta V)^2}{2 \times 3600} \qquad \text{(S6)}$$

ΔV is the potential window used.

Specific Power (P_s in W kg^{-1})

$$P_s = \frac{E}{t_d} \times 3600 \qquad \text{(S7)}$$

where, t_d is the discharge time at constant current.

Coulombic effecieny (η in %)

$$\eta(\%) = \frac{t_d}{t_c} \times 100 \qquad \text{(S8)}$$

where, t_c and t_d are the charging and discharge times (in s).

b-value and its significance

$$i_p = a\upsilon^b \qquad \text{(S9)}$$

i_p is peak current (A), υ is the scan rate mV s^{-1}, and a and b are fitting parameters. The b value is determined from the slope of the plot of log i_p *vs*. log scan rate. The b ~0.5 indicates the faradaic intercalation process, and the b = 1 indicates the capacitive process [6].

Capacitance (C in F) from electrochemical impedance spectroscopy

$$C = \frac{-1}{2\pi f Z''} \qquad \text{(S10)}$$

where, f is the frequency (Hz) and Z'' is the imaginary part of the impedance (Ω).

S4. *Descriptions of electrical elements involved in equivalent circuit*

$R_s(R_{ct}Q_1)((R_{leak}C_{dl})(Q_2))W$

The electrical elements involved are solution resistance (R_s) - a resistance that emerges from the electrolyte used, charge-transfer resistance (R_{ct}) - the resistance against the transport of charges across electrolyte and electrode material, and across electrode materials and current collector, leakage resistance (R_{leak}) - the resistance due to loss of potential from the system when not connected with an external circuit or a load, Warburg diffusion resistance (W) - the resistance against the diffusion of electrolyte ions into the electrode material, the electrical

double layer capacitance (C_{dl}) at the interface between the electrode material and electrolyte, constant phase elements (Q_1 and Q_2). Q_1 and Q_2 are used in place of the ideal capacitors C_1 and C_2 because the rough surface of the electrode material causes frequency dispersion during the measurement, causing the depressed semicircle at high-frequency region instead of a perfect semicircle, thereby making the capacitor to deviate from its ideality. The ideal capacitor is related to the constant phase element by the following Eqn. (S11),

$$C = Q(\omega_{max})^{n-1} \quad \text{(S11)}$$

where ω_{max}, is the frequency corresponding to the maximum of the imaginary part (Z'') and n is the roughness factor (n = 0, ideal resistor, n = +1, ideal capacitor), which is a measure of the surface inhomogeneity of the electrode material [7] ($n_1 = 0.99$ and $n_2 = 0.52$).

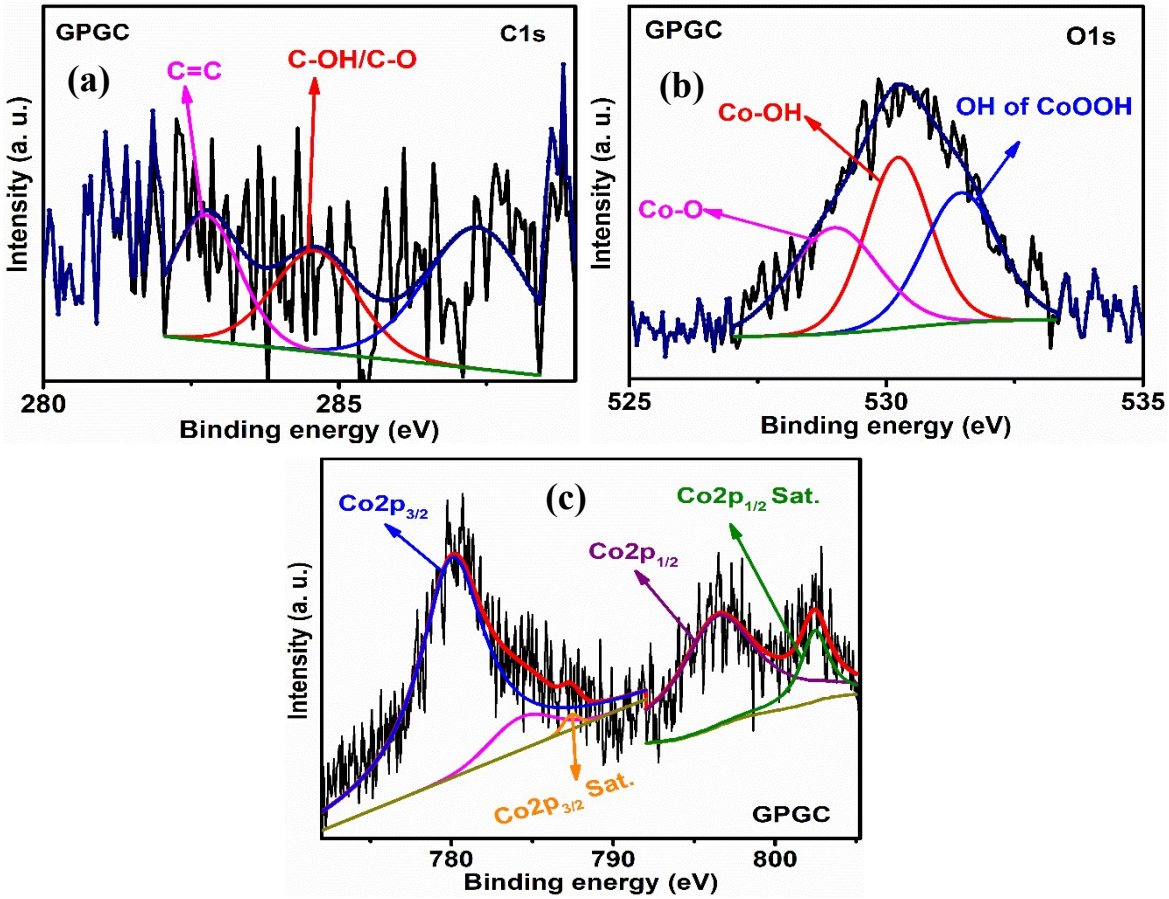

Fig. S1 core level spectra of (a) C 1s, (b) O 1s and (c) Co 2p

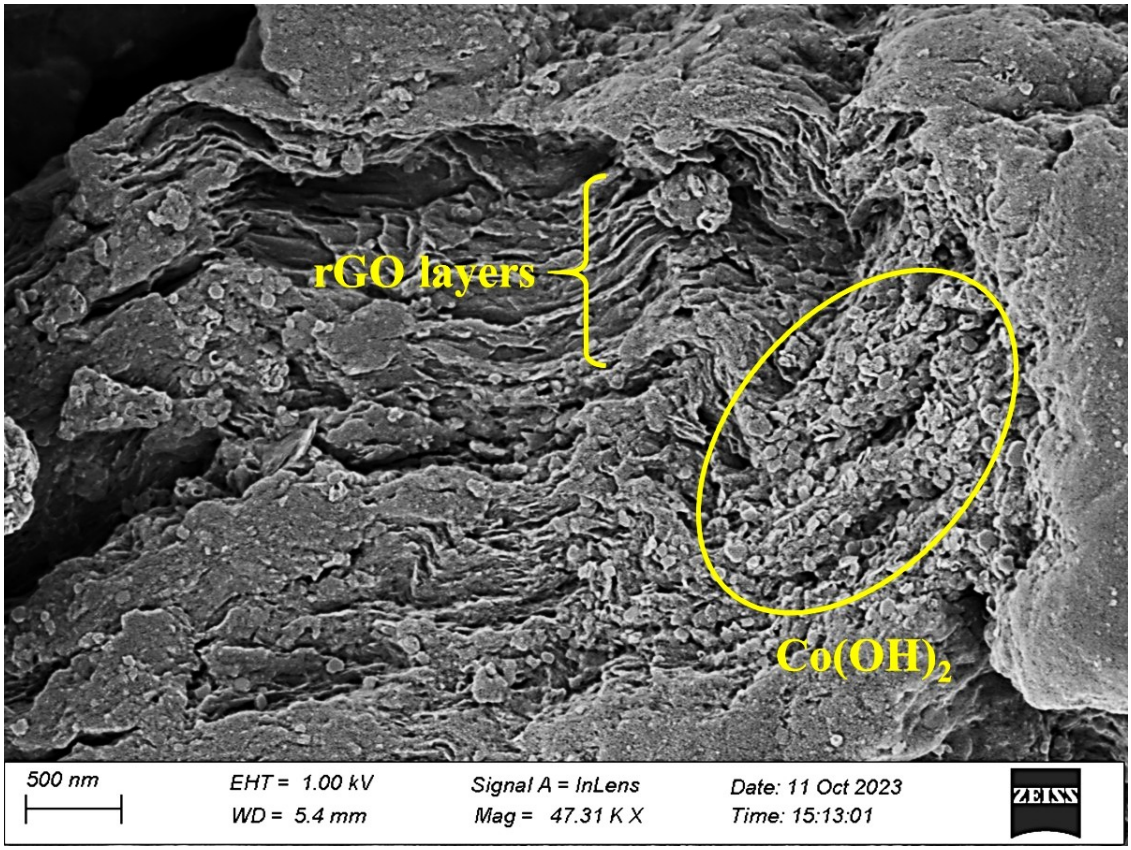

Fig. S2 FE-SEM image of GC with its constituents marked.

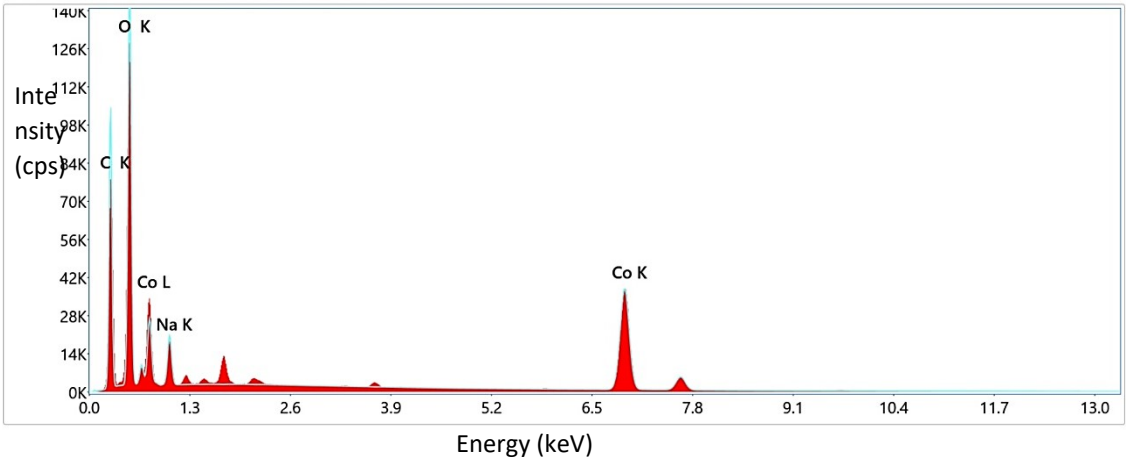

Fig. S3 The energy dispersive spectrum (EDS) of GC.

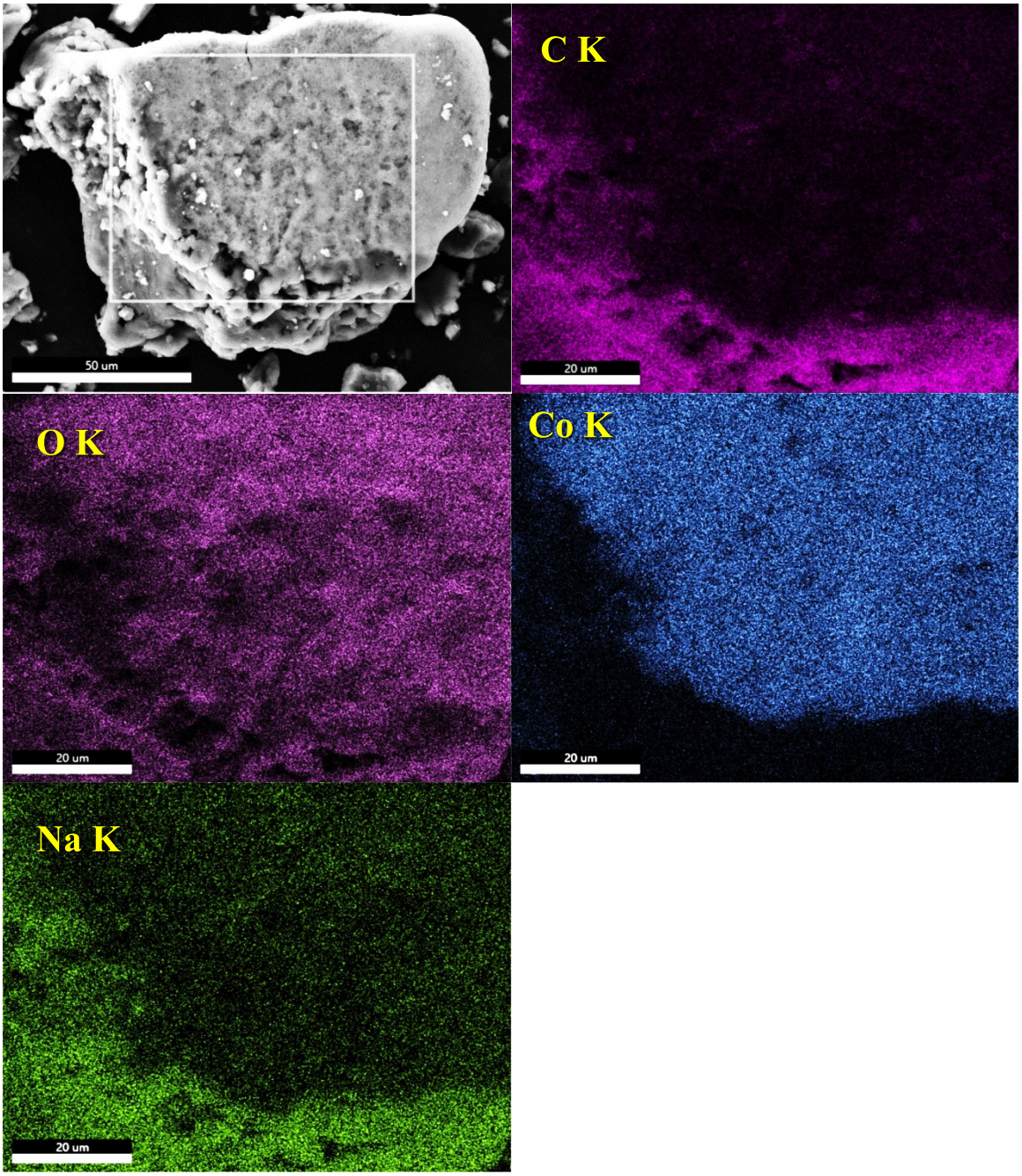

Fig. S4 The elemental maps of GC obtained using the EDS attached to the FE-SEM instrument.

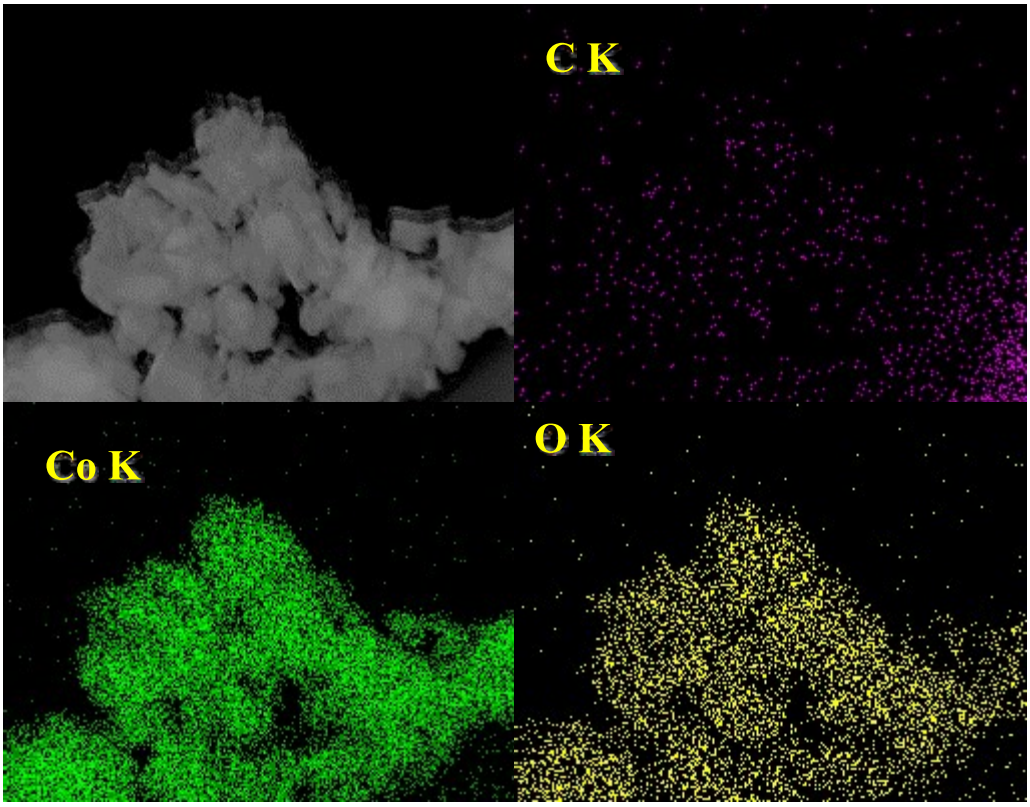

Fig. S5 The elemental maps of GC were obtained using the EDS attached to the TEM instrument.

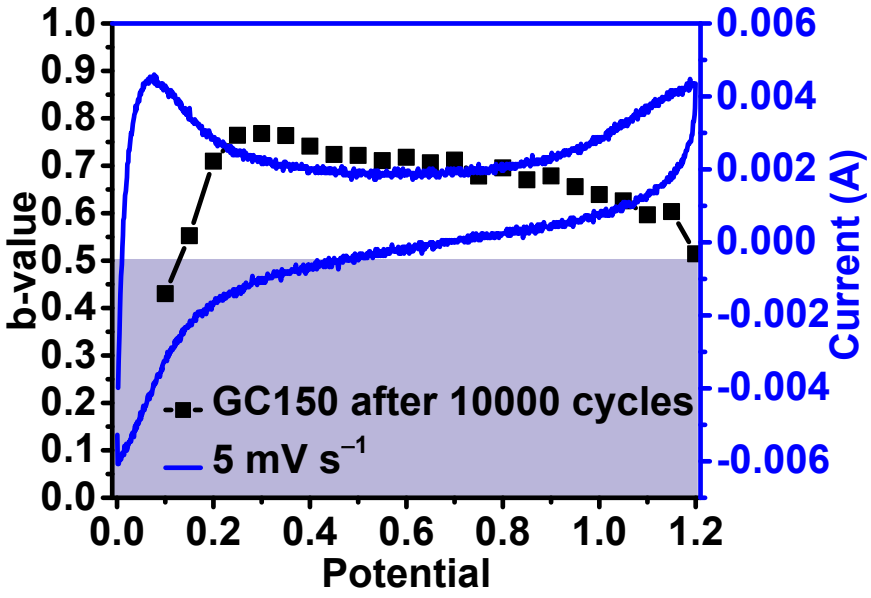

Fig. S6 The plots of b-value *vs*. potenital and CV plot at scan rate of 5 mV s^{-1} of GC150

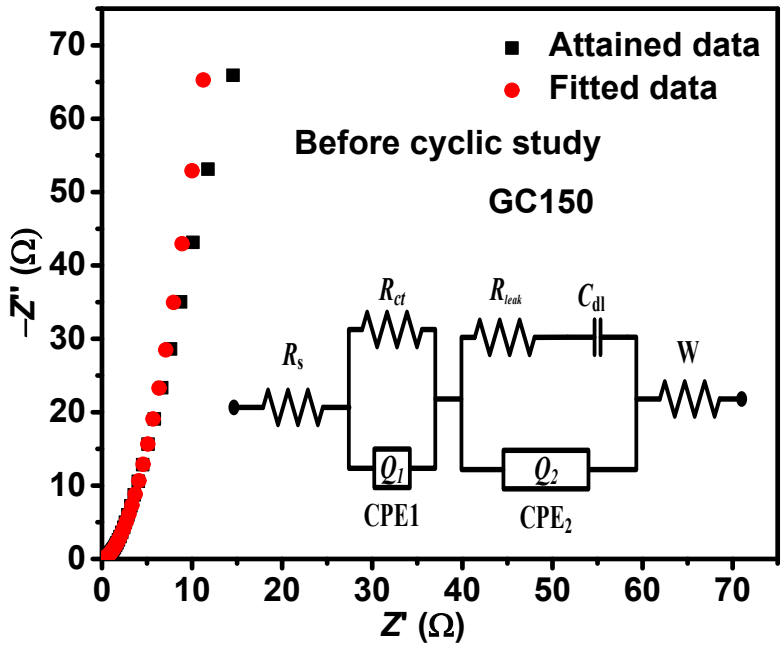

Fig. S7 The attained and fitted Nyquist plots of GC150 using the equivalent circuit of $R_s(R_{ct}Q_1)((R_{leak}C_{dl})(Q_2))W$

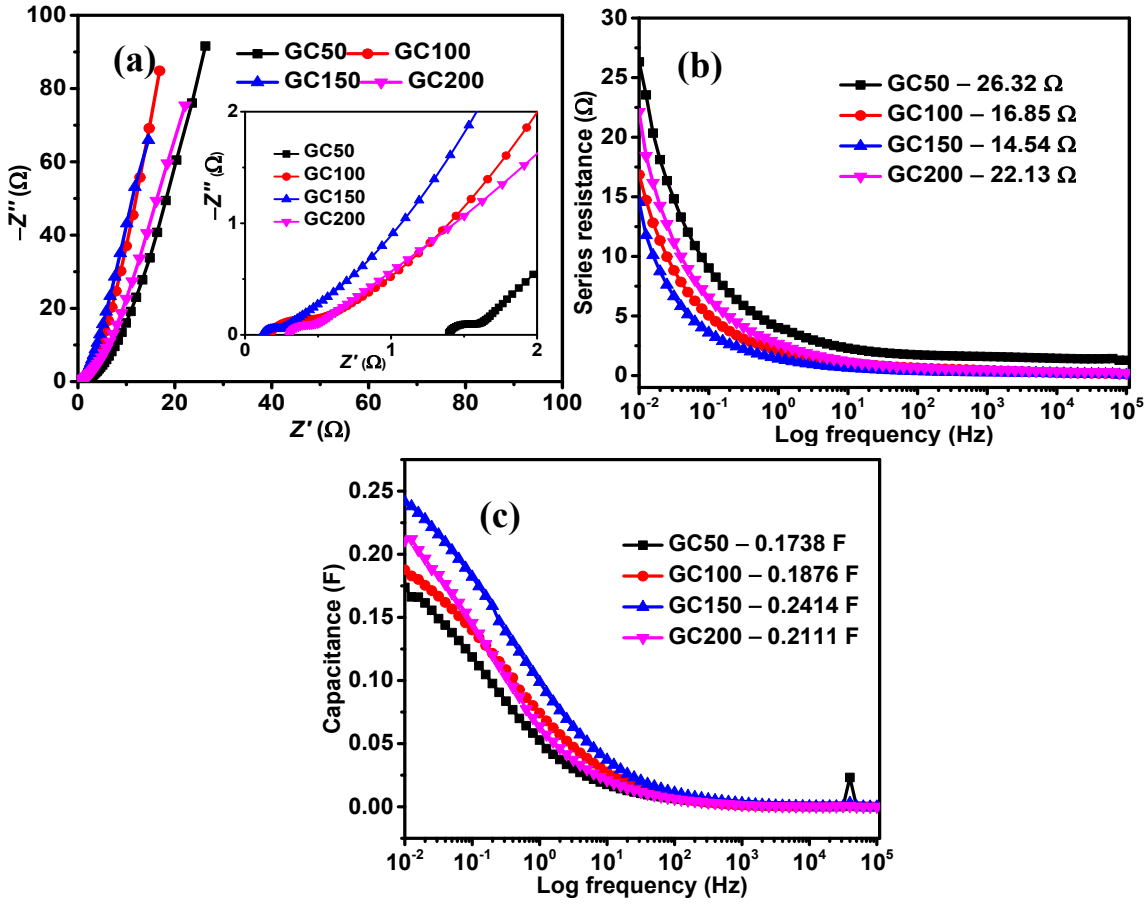

Fig. S8 a) Nyquist plots, plots of b) series resistance *vs*. log frequency, c) capacitance *vs*. log frequency of GC composites.

Table S1 weight and atomic percentages of elements of GC150

Element	Weight %	Atomic %
C K	47.0	60.0
O K	36.0	34.6
Na K	2.4	1.6
Co K	14.6	3.8

Table S2 The magnitudes of electrical parameters of GC composites obtained by equivalent circuit fitment.

composite	R_s (Ω)	R_{ct} (Ω)	Q_1 (F)	n_1	R_{leak}	C_{dl}	Q_2	n_2	W
GC50	1.024	0.8924	0.1650	0.7800	0.5288	0.217	0.0037	0.46	0.1406
GC100	0.0115	0.4871	0.0192	0.5037	0.0936	0.2324	1.555	0.9	0.1907
GC150	0.0100	0.1489	0.0308	0.6609	0.2300	0.2865	0.0016	0.64	0.2703
GC200	0.1986	1.159	0.1501	0.4500	0.0204	0.2668	0.0037	0.6144	6.883

References

[1] D.C. Marcano, D.V. Kosynkin, J.M. Berlin, A. Sinitskii, Z. Sun, A. Slesarev, L.B. Alemany, W. Lu, J.M. Tour, Improved Synthesis of Graphene Oxide, ACS Nano. 4 (2010) 4806–4814. https://doi.org/10.1021/nn1006368.

[2] R. Sharma, N. Chadha, P. Saini, Determination of defect density, crystallite size and number of graphene layers in graphene analogues using X-ray diffraction and Raman spectroscopy, Indian J. Pure Appl. Phys. 55 (2017) 625–629.

[3] A. Viswanathan, A.N. Shetty, Reduced graphene oxide/vanadium pentoxide nanocomposite as electrode material for highly rate capable and durable supercapacitors, J. Energy Storage. 27 (2020) 101103. https://doi.org/10.1016/j.est.2019.101103.

[4] M.D. Stoller, R.S. Ruoff, Best practice methods for determining an electrode material's performance for ultracapacitors, Energy Environ. Sci. 3 (2010) 1294. https://doi.org/10.1039/c0ee00074d.

[5] G. Nyström, A. Marais, E. Karabulut, L. Wågberg, Y. Cui, M.M. Hamedi, Self-assembled three-dimensional and compressible interdigitated thin-film supercapacitors and batteries, Nat. Commun. 6 (2015) 7259. https://doi.org/10.1038/ncomms8259.

[6] J. Wang, J. Polleux, J. Lim, B. Dunn, Pseudocapacitive Contributions to Electrochemical Energy Storage in TiO2 (Anatase) Nanoparticles, J. Phys. Chem. C. 111 (2007) 14925–14931. https://doi.org/10.1021/jp074464w.

[7] N. Dinodi, A.N. Shetty, Alkyl carboxylates as efficient and green inhibitors of magnesium alloy ze41 corrosion in aqueous salt solution, Corros. Sci. 85 (2014) 411–427. https://doi.org/10.1016/j.corsci.2014.04.052.